JOURNAL OF PROPULSION AND POWER
Vol. 27, No. 3, May–June 2011

Technical Notes

Multiobjective Optimization of Circumferential Casing Grooves for a Transonic Axial Compressor

Jin-Hyuk Kim,* Kwang-Jin Choi,* Afzal Husain,† and Kwang-Yong Kim‡
Inha University, Incheon 402-751, Republic of Korea

DOI: 10.2514/1.50563

Nomenclature

C	=	tip chord length of the blade
D	=	depth of the grooves
m	=	mass flow rate
P_t	=	total pressure
T_t	=	total temperature
W	=	width of the grooves
γ	=	specific heat ratio
η_{peak}	=	peak adiabatic efficiency

Subscripts

in, out	=	inlet and outlet, respectively
peak, stall	=	peak adiabatic efficiency point and near stall point, respectively

I. Introduction

RECENTLY, casing treatments using grooves or slots have been applied to axial compressors to prevent surge and enhance stall margin (SM). However, this is accompanied by a loss near the blade tip region, which leads to a decrease in efficiency of the axial compressor. Therefore, a systematic design of the casing treatment using multiobjective optimization techniques in conjunction with a flow analysis using three-dimensional Reynolds-averaged Navier–Stokes equations (RANS) was used to investigate a compromise between the SM and the efficiency of the compressor.

Various types of grooves have been suggested by many researchers, and it has been reported that using grooves increases SM by delaying stall. Huang et al. [1] studied the effects of the configuration, width, and depth of circumferential groove casing treatment on SM by numerical analysis, and suggested that the stall mechanism was substantially influenced by tip clearance. Muller et al. [2] studied the effects of the number and depth of the grooves on SM by three-dimensional numerical analysis. Houghton and Day [3] examined the effect of grooves on rotor outflow blockage, and the near casing flowfield was studied using experimental and computational methods.

Many engineering designs involve multiple disciplines and simultaneous optimization of multiple objectives related to each discipline. These design problems, usually known as multiobjective problems, require simultaneous consideration of all objective functions to optimize the system. The nondominated sorting genetic algorithm (NSGA-2) by Deb [4] generates a Pareto-optimal solution using an evolutionary algorithm. Shape optimization of a hydraulic turbine diffuser was performed with multiple objectives by Marjavaara et al. [5]. Kim et al. [6] reported a multiobjective optimization of a centrifugal compressor impeller with four design variables that defined the impeller hub and shroud contours in meridian terms. Samad and Kim [7] reviewed the performance of the surrogate models applied to turbomachinery design optimization, and introduced multi and single-objective optimization techniques in conjunction with three-dimensional RANS analysis.

In this study, based on previous work [8] for a single-objective optimization, a hybrid multiobjective evolutionary algorithm (hybrid MOEA) [9] coupled with the Kriging (KRG) model [10] was applied to obtain a global Pareto-optimal front for the design of circumferential casing grooves in an axial compressor with NASA Rotor 37 [11]. To the best of the authors' knowledge, no previous study has reported on the optimization of the design of circumferential casing grooves. The present multiobjective optimization was motivated to provide an efficient tool for the design of an axial compressor with circumferential casing groove treatment, and it is expected for designers to meet their design requirements with regard to the SM and adiabatic efficiency from the Pareto-optimal designs (PODs) obtained in this work. Numerical solutions at the selected design points were obtained by three-dimensional RANS analysis. The shape of the grooves was optimized by considering width and depth as design variables in order to improve the SM and the peak adiabatic efficiency. The tradeoff between these two competing objective functions is explored and discussed with respect to the design variables.

II. Problem Description and Numerical Analysis

The compressor model investigated in this study is a transonic axial compressor with NASA Rotor 37 [11]. The rotor operates at a speed of 17,188.7 rpm, the total pressure ratio is 2.106, and the adiabatic efficiency is 88.9% at 20.19 kg/s. The blade of NASA Rotor 37 sections is defined by a multiple-circular arc. The tip clearance is 0.356 mm (0.47% span), the choking mass flow is 20.93 kg/s, and the near stall point is 0.925 of the choke flow. Flow parameters such as total pressure and total temperature in relation to mass flow rate were measured at the inlet and the outlet located 41.9 mm upstream of the blade leading edge and 106.7 mm downstream of the trailing edge near the hub, respectively.

For the flow analysis, a steady-state three-dimensional simulation of a transonic axial compressor with circumferential casing grooves was performed using the finite volume solver ANSYS-CFX. Also, Blade-Gen, Turbo-Grid, CFX-Pre, CFX-Solver, and CFX-Post were used to create the blade profile, generate the computational mesh, define the boundary conditions, and perform flow analysis and postprocessing, respectively. three-dimensional RANS equations with the shear stress transport (SST) turbulence model [12] were discretized using finite volume approximations. In this study, the near wall grid resolution was adjusted to keep $y^+ < 2$ to implement low Reynolds number version of the SST model.

The computation domain consisted of one passage of an axial compressor rotor and five circumferential casing grooves. The one passage had O-type grids near the blade surfaces and H/J/C/L grids in other regions. The inlet and outlet blocks were constructed with $60 \times 37 \times 17$ and $60 \times 37 \times 21$ grid points, respectively, while the main passage (except for the tip clearance and the O-type grids) was constructed with $40 \times 37 \times 84$ grid points. The tip clearance and

Received 29 April 2010; revision received 13 October 2010; accepted for publication 28 November 2010.

*Graduate Student, Department of Mechanical Engineering.
†Full-Time Lecturer, Department of Mechanical Engineering.
‡Professor, Department of Mechanical Engineering; kykim@inha.ac.kr. Associate Fellow AIAA (Corresponding Author).

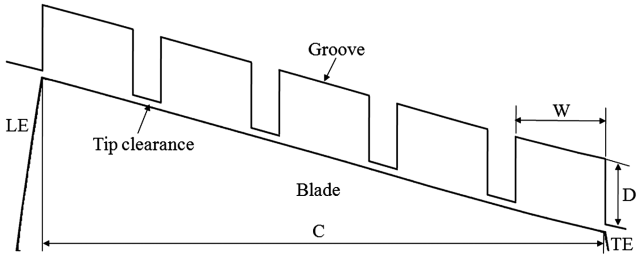

Fig. 1 Definition of the design variables.

O-type grids were constructed with $20 \times 37 \times 84$ and 216,720 grid points, respectively. O-type grids with a width factor of 0.5 and 20 elements were assigned. The grid-independency test has been carried out, and a total of 480,000 grid points were used for the flow analysis of the compressor. Each groove was constructed with $20 \times 48 \times 25$ grid points. Ideal gas was used as the working fluid. The total pressure and total temperature at the inlet were set to 101,325 Pa and 288.15 K, respectively. The designed mass flow rate was set at the outlet for steady-state simulation. The solid boundaries were assumed as hydraulically smooth and assigned adiabatic and no-slip boundary conditions. A periodic boundary was used along the passage. The connection between the passage and the groove was made using the general grid interface method, which is a grid connection approach used when the grids on either side of connected surfaces do not match.

The computations were performed by an Intel Core I7 CPU 2.67 GHz PC. The computational time was about 6–7 h depending on the mesh size of the geometry.

III. Optimization Procedure

In the optimization procedure, initially, based on the problem definition, the objective function was determined, and the design variables and design spaces were selected through parametric and sensitivity studies. Next, using design of experiment techniques, the design points were selected. The objective function values at these design points were evaluated by RANS analyses. The results were used to construct the surrogate model and to generate a global Pareto-optimal front for multiobjective optimization.

The objective of our optimization problem was to maximize both the SM and the peak adiabatic efficiency (η_{peak}), which were selected as objective functions for the shape optimization of the circumferential casing grooves. These objective functions are defined as follows:

$$\text{SM} = \left(\frac{m_{\text{peak}}}{m_{\text{stall}}} \times \frac{\text{PR}_{\text{stall}}}{\text{PR}_{\text{peak}}} - 1\right) \times 100\% \tag{1}$$

$$\eta_{\text{peak}} = \frac{\left(\frac{P_{t,\text{out}}}{P_{t,\text{in}}}\right)^{\frac{\gamma-1}{\gamma}} - 1}{\left(\frac{T_{t,\text{out}}}{T_{t,\text{in}}}\right) - 1} \tag{2}$$

To find the stall inception point, the normalized mass flow rate was reduced step by step with a decrement of 0.01 until the solution did not converge. The last converged point was considered to be the near stall point. The following convergence criteria were suggested by Chen et al. [13]:

1) The inlet mass flow rate variation is less than 0.001 kg/s for 300 steps.

Table 1 Design space

Variables	Lower bound	Upper bound
D/C	0.077	0.231
W/C	0.120	0.192

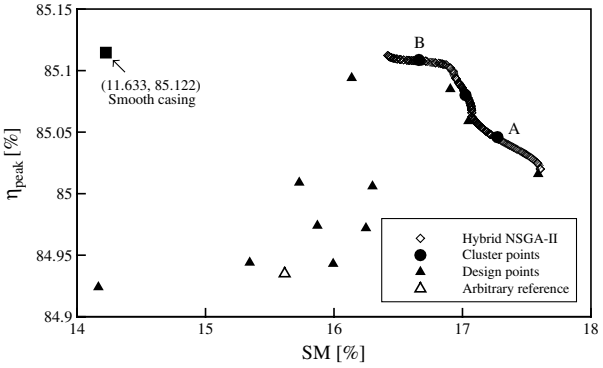

Fig. 2 Pareto-optimal solutions with representative PODs A and B and distribution of the objective function values at design points.

2) The difference between the inlet and outlet mass flow rate is less than 0.5%.

3) At that time, the adiabatic efficiency variation is less than 0.3% per 100 steps.

The same convergence criteria were used to find the numerical stall inception point in this work. To maximize the two objectives simultaneously, a hybrid MOEA coupled with a RANS analysis was applied to obtain Pareto-optimal solutions.

Circumferential casing grooves improve the SM and the operating range of a transonic axial compressor, and the SM is influenced by the geometry of the grooves as reported by many researchers. Huang et al. [1] tested the effect of groove width, from 5 to 12% of the tip chord, on compressor performance. Their test results suggested that the SM improvement increased as the groove width increased, and a large width was recommended. Bailey [14] performed an experiment on the effects of the location, the groove depth, and the number of grooves in a single-stage axial compressor. Depths of 0.381, 1.143, and 2.896 cm were tested with fixed width and spacing between grooves. Their results show that increasing the depth of the circumferential grooves resulted in increased SM and no significant effect on efficiency.

In our study, the geometric parameters defining the circumferential casing grooves were selected as optimization design variables. The flowfield near the tip region is very complex, sensitive to the efficiency and pressure, and influenced by the geometry around the tip region. Thus, as shown in Fig. 1, the depth (D) and the width (W) of the grooves normalized by the tip chord length (C); i.e., W/C and D/C, were selected to change the groove shape for the purpose of controlling the flowfield near the tip region. The groove geometry was varied by changing the width and the depth within the design space set by the preliminary computation. The grooves were evenly located with the same gap between grooves from the leading edge to the trailing edge.

For design optimization, it is important to find the feasible and practical design space that is formed by setting up the ranges of the design variables. The range of our design variables is presented in Table 1. The upper range of the groove width was determined such that five grooves could not overlap each other within the tip chord length. The range of groove depth was determined through preliminary computations. Design points within the design space were selected with the help of Latin hypercube sampling as design of experiment [15]. And, the KRG model [10], also known as a KRG metamodel, was used as a deterministic technique for optimization.

Table 2 Design variables corresponding to the optimal clusters from the global Pareto-optimal solutions

Designs	Design Variables	
	D/C	W/C
Reference design	0.088	0.192
POD A	0.150	0.133
POD B	0.077	0.131

Table 3 Objective function values at the Pareto-optimal solutions from global Pareto-optimal solutions

Designs	MOEA prediction		RANS		Improvement, %	
	SM	η_{peak}	SM	η_{peak}	SM	η_{peak}
Smooth casing	——	——	11.633	85.122	——	——
Reference design	——	——	15.616	84.935	——	——
POD A	17.272	85.046	17.300	85.041	10.784	0.125
POD B	16.661	85.109	15.804	85.099	1.204	0.193

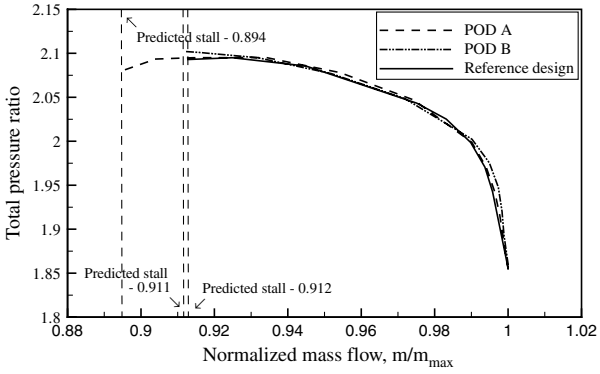

a) Total pressure ratio

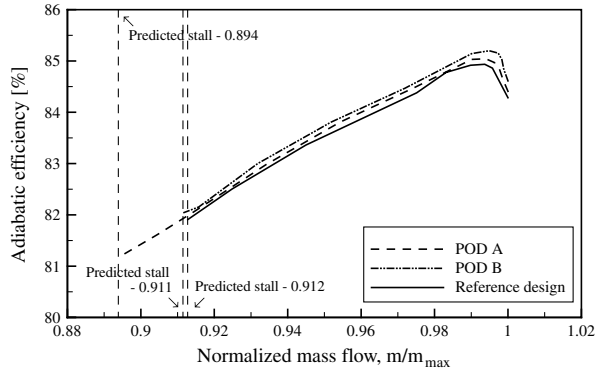

b) Adiabatic efficiency

Fig. 3 Performance curves for the optimal and reference designs.

In this study, a hybrid MOEA [9] was used to obtain global Pareto-optimal solutions for the multiobjective optimization problem. In this method, first, approximate Pareto-optimal solutions were obtained using real coded NSGA-2 [16] for two objective functions. Here, real coded means that the crossover and mutations were conducted in real space to obtain a response of NSGA-2. These solutions were then refined by searching a local optimal solution for each objective function over all NSGA-2-obtained optimal solutions using sequential quadratic programming with NSGA-2 solutions as initial guesses. In the present study, one objective was optimized, treating the others as equality constraints, and the local search was repeated for the second objective function, treating the first as an equality constraint [9]. This process gave rise to two new sets of optimal solutions that were merged with the NSGA-2 solutions. From these solutions, the first dominated solution was discarded, and then duplicate solutions were removed to obtain global Pareto-optimal solutions. The process of local search improved the quality of the Pareto-optimal solutions. The functional representation of the global Pareto-optimal solutions is called the Pareto-optimal front. To find representative solutions from the global Pareto-optimal solutions, these solutions were grouped into user-defined clusters by applying *K*-means clustering [15].

IV. Results and Discussion

The numerical results of the flow analysis were validated using experimental data [17] in the previous work [8]. The measured near stall point was 0.925 which is the mass flow normalized by choking mass flow, and the predicted near stall point based on the convergence criterion was 0.921.

Figure 2 shows the global Pareto-optimal solutions that were generated by a hybrid MOEA through the surrogate model along the data points. Since both objective functions were maximized, the Pareto-optimal solution resembles a convex front. The tradeoff analysis shows that higher peak adiabatic efficiency can be obtained at the cost of lower SM and vice versa. Two representative PODs were selected through *K*-means clustering as shown in Fig. 2 and

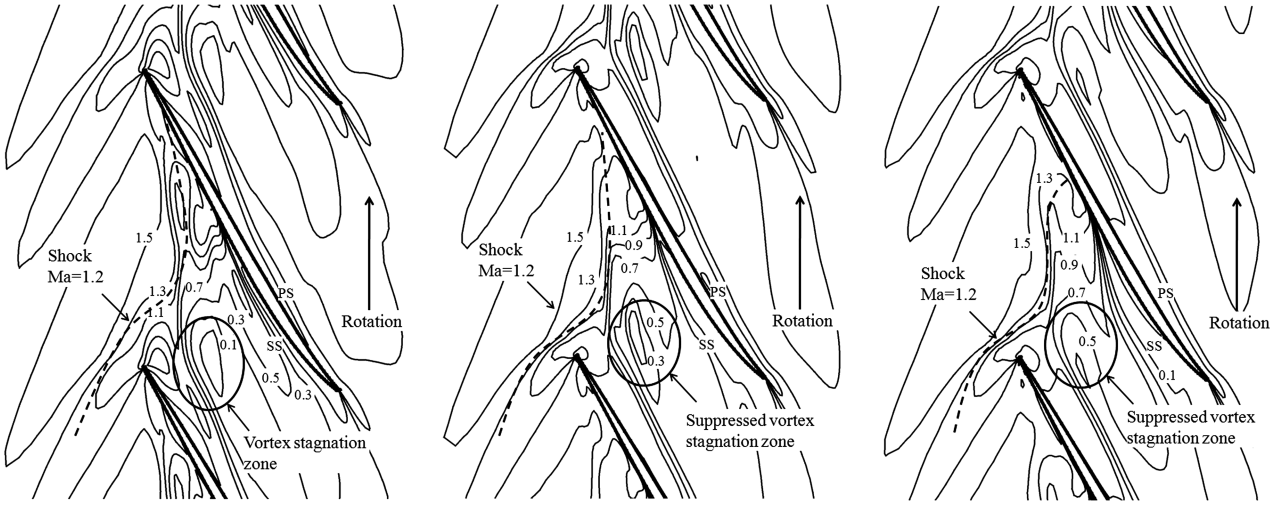

a) Reference design **b) POD A** **c) POD B**

Fig. 4 Mach number contours for the reference design, POD A, and POD B at the near stall point of the reference design (98% span): a) reference design, b) POD A, and c) POD B.

Table 2. These designs were reproduced through RANS analysis and compared with the reference design as shown in Table 3. An arbitrary geometry was selected among the various design points as the reference design. As shown in Fig. 2, POD A represents high SM with low efficiency. On the other hand, POD B represents low SM with high efficiency.

Both PODs, A and B, are superior to the reference design for both objectives. POD A and B show improvements in SM of 10.784 and 1.204%, respectively, and improvements in peak adiabatic efficiency by 0.125 and 0.193%, respectively, compared with the reference design. However, when compared with the smooth casing design, the PODs show a much larger SM and a slightly lower peak adiabatic efficiency.

Figures 3a and 3b indicate the total pressure ratio and the adiabatic efficiency, respectively, for the reference design, POD A, and POD B. As shown in these figures, the near stall points of PODs A and B were predicted to be 0.894 and 0.911, respectively. The total pressure ratios of PODs A and B are 2.079 and 2.102, respectively. The adiabatic efficiency of PODs A and B at the peak adiabatic efficiency points are 85.041 and 85.099%, respectively. These results show that the optimum shape of POD A has the highest SM whereas the optimum shape of POD B has the highest peak adiabatic efficiency. Also, the SM and peak adiabatic efficiency were shown to be further increased by the optimization compared with the reference design.

Figure 4 indicates Mach number contours at 98% span of the reference design, and PODs A and B at the near stall point of the reference design (normalized mass flow, 0.912). As shown in Fig. 4, interaction between the tip leakage vortex and the passage shock resulted in a large low-speed region downstream of the interaction. This low-energy region is the vortex stagnation zone that changed the main flow and led to a separation by increasing the back pressure. The flow in the vortex stagnation zone was almost circumferential, with a negligible axial velocity component. We found that this stagnation zone was suppressed largely by the optimization, as shown in Figs. 4b and 4c for PODs A and B, respectively.

V. Conclusions

Multiobjective optimization of circumferential casing grooves in a transonic axial compressor was performed using a KRG model and genetic algorithm with three-dimensional RANS analysis to obtain a global Pareto-optimal front. It was found that two selected representative PODs, A and B, were superior to the reference design for both the SM and the peak adiabatic efficiency. The flowfields of the reference design, POD A, and POD B were analyzed to understand the effect of the multiobjective optimization. By the optimization, the stagnation zone was decreased at the near stall point of the reference design, which led to an extension of the stable operating range. Improvement in peak adiabatic efficiency was achieved by repositioning the tip leakage vortex closer to the pressure surface of the blade.

Acknowledgment

This research was supported by an Inha University Research Grant.

References

[1] Huang, X., Chen, H., and Fu, S., "CFD Investigation on the Circumferential Grooves Casing Treatment of Transonic Compressor," ASME Turbo Expo, ASME Rept. GT2008-51107, Berlin, 2008.

[2] Muller, M. W., Schiffer, H. P., and Hah, C., "Effect of Circumferential Grooves on the Aerodynamic Performance of an Axial Single-Stage Transonic Compressor," ASME Turbo Expo, ASME Rept. GT2007-27365, Montreal, 2007.

[3] Houghton, T., and Day, I., "Enhancing the Stability of Subsonic Compressors Using Casing Grooves," ASME Turbo Expo, ASME Rept. GT2009-59210, Orlando, FL, 2009.

[4] Deb, K., *Multiobjective Optimization Using Evolutionary Algorithms*, 1st ed., Wiley, Chichester, England, U.K., 2001.

[5] Marjavaara, B. D., Lundstrom, T. S., Goel, T., Mack, Y., and Shyy, W., "Hydraulic Turbine Diffuser Shape Optimization by Multiple Surrogate Model Approximations of Pareto Fronts," *Journal of Fluids Engineering*, Vol. 129, No. 9, 2007, pp. 1228–1240. doi:10.1115/1.2754324

[6] Kim, J. H., Choi, J. H., Husain, A., and Kim, K. Y., "Multiobjective Optimization of a Centrifugal Compressor Impeller Through Evolutionary Algorithms," *Journal of Power and Energy*, Vol. 224, No. 5, 2010, pp. 711–721. doi:10.1243/09576509JPE884

[7] Samad, A., and Kim, K. Y., "Surrogate Based Optimization Techniques for Aerodynamic Design of Turbomachinery," *International Journal of Fluid Machinery and Systems*, Vol. 2, No. 2, 2009, pp. 179–188.

[8] Choi, K. J., Kim, J. H., and Kim, K. Y., "Design Optimization of Circumferential Casing Grooves for a Transonic Axial Compressor to Enhance Stall Margin," ASME Turbo Expo, ASME Rept. GT2010-22396, Glasgow, Scotland, U.K., 2010.

[9] Deb, K., and Goel, T., "A Hybrid Multiobjective Evolutionary Approach to Engineering Shape Design," *Proceedings of Evolutionary Multicriterion Optimization Conference*, Zurich, 2001, pp. 385–399.

[10] Martin, J. D., and Simpson, T. W., "Use of Kriging Models to Approximate Deterministic Computer Models," *AIAA Journal*, Vol. 43, No. 4, 2005, pp. 853–863. doi:10.2514/1.8650

[11] Reid, L., and Moore, R. D., "Design and Overall Performance of Four Highly-Loaded, High-Speed Inlet Stage for an Advanced, High-Pressure-Ratio Core Compressor," NASA TP-1337, 1978.

[12] Menter, F. R., "Two-Equation Eddy-Viscosity Turbulence Models for Engineering Applications," *AIAA Journal*, Vol. 32, No. 8, 1994, pp. 1598–1605. doi:10.2514/3.12149

[13] Chen, H., Huang, X., and Fu, S., "CFD Investigation on Stall Mechanisms and Casing Treatment of a Transonic Compressor," 42nd AIAA/ASME/SAE/ASEE Joint Propulsion Conference and Exhibit, AIAA Paper 2006-4799, Sacramento, CA, 2006.

[14] Bailey, E. E., "Effect of Grooved Casing Treatment on the Flow Range Capability of a Single-Stage Axial-Flow Compressor," NASA TM X-2459, 1972.

[15] JMP, The Statistical Discovery Software, Ver. 6, SAS Institute, Cary, NC, 2005.

[16] Deb, K., Agrawal, S., Pratap, A., and Meyarivan, T., "A Fast and Elitist Multi-Objective Genetic Algorithm for Multi-Objective Optimization: NSGA-2," *Proceedings of the Parallel Problem Solving from Nature 6 Conference*, Paris, 2000, pp. 849–858.

[17] Dunham, J., "CFD Validation for Propulsion System Components," AGARD Advisory Rept. 355, 1998.

R. Miller
Associate Editor